iScience

CellPress
OPEN ACCESS

Article

A meiotic switch in lysosome activity supports spermatocyte development in young flies but collapses with age

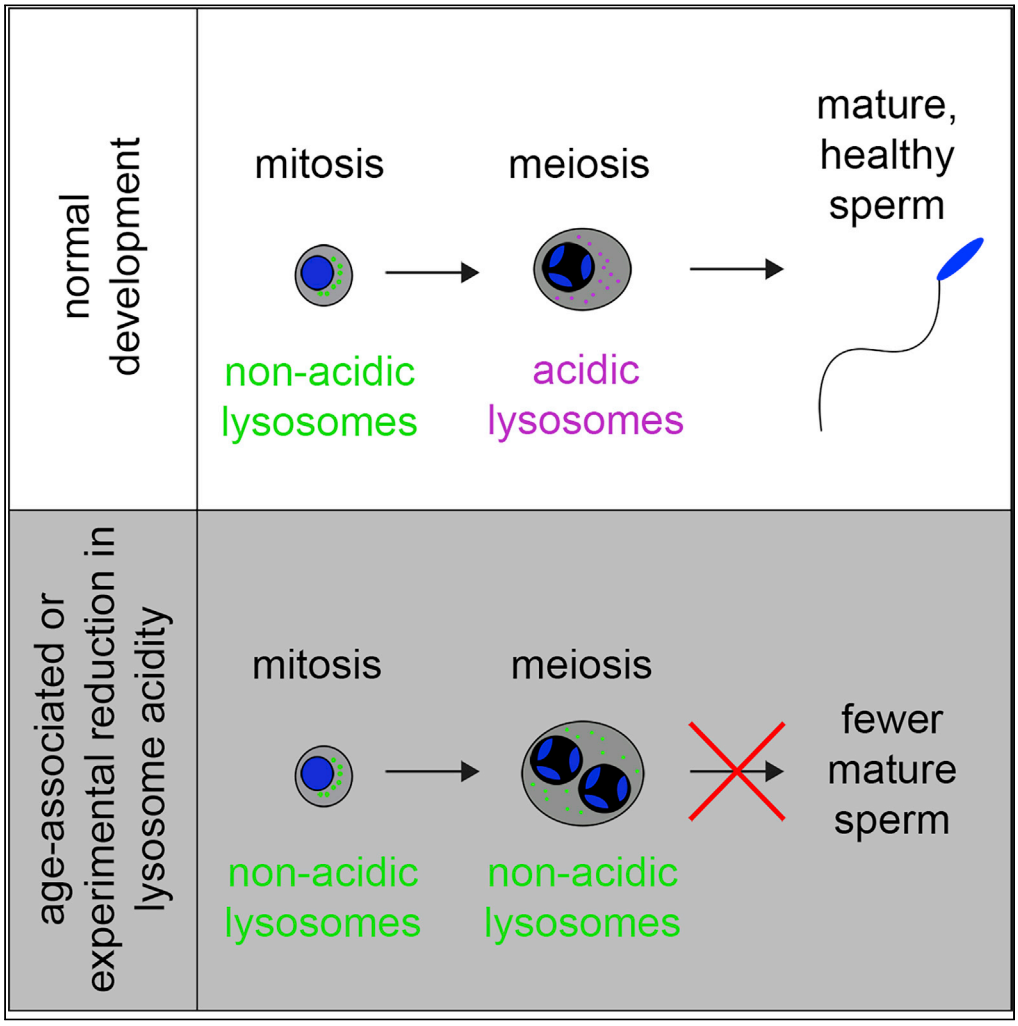

Tyler J. Butsch, Olga Dubuisson, Alyssa E. Johnson, K. Adam Bohnert

bohnerta@lsu.edu

Highlights

Lysosomes acidify at the mitotic-meiotic transition in the testis

Acidic lysosomes support germ-cell membrane stability

Lysosome acidity naturally declines in the aging male germline

Lysosome acidification is required for mature sperm production

Butsch et al., iScience *25*, 104382
June 17, 2022
https://doi.org/10.1016/j.isci.2022.104382

iScience

CellPress
OPEN ACCESS

Article

A meiotic switch in lysosome activity supports spermatocyte development in young flies but collapses with age

Tyler J. Butsch,[1] Olga Dubuisson,[1] Alyssa E. Johnson,[1] and K. Adam Bohnert[1,2,*]

SUMMARY

Gamete development ultimately influences animal fertility. Identifying mechanisms that direct gametogenesis, and how they deteriorate with age, may inform ways to combat infertility. Recently, we found that lysosomes acidify during oocyte maturation in *Caenorhabditis elegans*, suggesting that a meiotic switch in lysosome activity promotes female germ-cell health. Using *Drosophila melanogaster*, we report that lysosomes likewise acidify in male germ cells during meiosis. Inhibiting lysosomes in young-male testes causes E-cadherin accumulation and loss of germ-cell partitioning membranes. Notably, analogous changes occur naturally during aging; in older testes, a reduction in lysosome acidity precedes E-cadherin accumulation and membrane dissolution, suggesting one potential cause of age-related spermatocyte abnormalities. Consistent with lysosomes governing the production of mature sperm, germ cells with homozygous-null mutations in lysosome-acidifying machinery fail to survive through meiosis. Thus, lysosome activation is entrained to meiotic progression in developing sperm, as in oocytes, and lysosomal dysfunction may instigate male reproductive aging.

INTRODUCTION

Infertility affects approximately 60-80 million couples worldwide, and male-related issues account for nearly half of infertility cases (Kumar and Singh, 2015). To address modern concerns in reproductive health, researchers must gain a detailed understanding of how spermatogenesis, the process that produces male gametes, is regulated during the life of an animal. The steps of spermatogenesis are well-conserved from flies to mammals (Griswold, 2016; Hennig, 1992). In *Drosophila melanogaster*, germline stem cells at the apical tip of the testis initiate cell division in response to signals from the hub (Figure 1A). The resulting daughter cell then undergoes four mitotic divisions with incomplete cytokinesis, forming a cyst of 16 cells connected by intercellular bridges (Fuller, 1993). Once the mitotic divisions are complete, the nuclei of the cyst synchronously enter meiotic prophase (Figure 1A) (Fuller, 1998). In male flies, meiotic prophase lasts approximately 80-90 h (Fuller, 1998). This extended developmental stage is arguably the most important in spermatogenesis; high levels of transcription occur, and cells grow 25-fold as they prepare to differentiate (Fuller, 1998; Lin et al., 1996; White-Cooper et al., 1998). Importantly, several forms of male infertility may stem from defects in meiotic prophase (Meyer et al., 1992; Soderstrom and Suominen, 1980). Despite this significance, the essential cellular events integrated with early meiosis in the male germline have not been extensively described.

We recently reported that lysosomes, organelles that play diverse roles in cellular health and homeostasis (Ballabio and Bonifacino, 2020), acidify and become active during meiotic maturation in *C. elegans* oocytes (Bohnert and Kenyon, 2017). This meiotic switch in lysosome activity appears to clear molecular damage and reset oocyte homeostasis in preparation for fertilization (Bohnert and Kenyon, 2017). Though switches in lysosome activity are an emerging facet of many developmental transitions (Leeman et al., 2018; Villegas et al., 2019; Xie et al., 2019), it is currently unknown if such a switch exists in spermatogenesis. Lysosomes participate in the death of pre-meiotic spermatogonia (Chiang et al., 2017; Feng et al., 2018; Lu and Yamashita, 2017; Yacobi-Sharon et al., 2013; Yang and Yamashita, 2015). But, whether lysosomes also actively promote sperm health and development is unclear. Investigating the spatiotemporal regulation of lysosomes in the male germline may reveal previously unidentified controls on sperm development.

[1]Department of Biological Sciences, Louisiana State University, 202 Life Sciences Building, Baton Rouge, LA 70803, USA

[2]Lead contact

*Correspondence: bohnerta@lsu.edu

https://doi.org/10.1016/j.isci.2022.104382

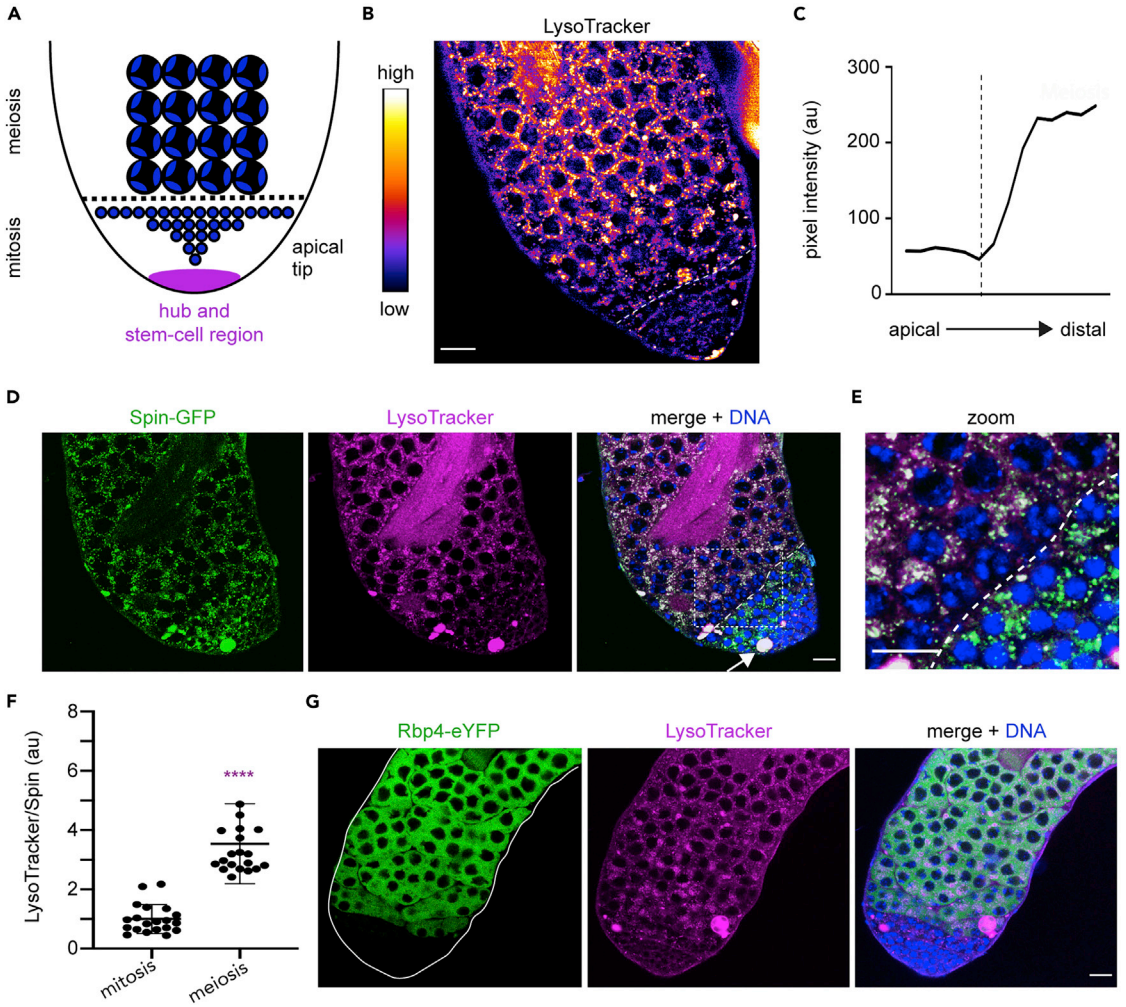

Figure 1. Lysosomes are robustly activated as *Drosophila* spermatocytes enter meiotic prophase

(A) Schematic of *Drosophila* spermatogenesis. Stem cells reside within the niche (the 'hub'; magenta) at the apical tip of the testis. Hub and stem cells are distinct but schematized together for simplicity. Near the tip, germline stem cells produce mitotic spermatogonia (solid blue dots). As they develop, germ cells push distally, and after four mitotic divisions, they enter meiosis (nuclei with three blue lobes).

(B) Heatmap of LysoTracker intensity in a live testis. The dashed line marks where LysoTracker intensity begins to increase.

(C) Plot of LysoTracker intensity from the apical tip to more distal regions.

(D) Spin-GFP (all lysosomes; driven by VasaGal4), LysoTracker (acidic lysosomes), and Hoechst (DNA) in a live testis. The arrow indicates dying spermatogonia.

(E) Merged image of outlined region from D. The dashed line separates mitotic and meiotic germ cells, based on nuclear morphology.

(F) Quantification of the ratio of LysoTracker to Spin-GFP intensity in mitotic (n = 20 testes) and meiotic (n = 20 testes) regions. Mean ± S.D. ****, $p < 0.0001$, Wilcoxon matched pairs signed rank test.

(G) Rbp4-eYFP (meiotic cells), LysoTracker (acidic lysosomes), and Hoechst (DNA) in a live testis. Bars, 20 μm. See also Figure S1.

Aging is a primary risk factor for infertility in both men and women (Harris et al., 2011; Ruman et al., 2003). Interestingly, lysosome acidity is known to be sensitive to aging in various cells and tissues (Baxi et al., 2017; Hughes and Gottschling, 2012). If this is also true in the animal germline, lysosome dysfunction may partly underlie age-related reproductive decline. A prominent cellular characteristic of old human testes is germ-cell multinucleation, an abnormality that arises when partitioning membranes between neighboring germ-cell nuclei break down (Holstein and Eckmann, 1986; Miething, 1993; Nistal et al., 1986; Paniagua et al., 1991). Molecularly, proper regulation of cell-adhesion molecules, such as E-cadherin (Ecad), may be necessary to balance membrane forces and prevent membrane dissolution at germ-cell boundaries (Kline et al., 2018; Loyer et al., 2015). Lysosomes are likely to feed into the regulation of Ecad localization and dynamics, as they have been shown to degrade Ecad in some biological contexts, including cancer metastasis

(Palacios et al., 2005; Wu and Hirsch, 2009). Deregulation of similar controls in the germline could potentiate changes to germ-cell membrane integrity and architecture, perhaps weakening cell boundaries and leading to reduced numbers of viable sperm.

In this study, we investigated the hypothesis that lysosomes promote healthy sperm development in *Drosophila*. We found that lysosomes acidify specifically in meiotic spermatocytes. Once active, lysosomes support membrane stability and prevent the loss of partitioning membranes that separate neighboring germ-cell nuclei. Our data suggest that lysosome-dependent downregulation of Ecad and potentially other membrane-associated molecules contribute to this function. We also provide evidence that lysosome acidity is diminished in testes from older animals. This age-related decrease in lysosome acidity correlates with developmental defects that mirror those seen upon pharmacological and genetic inhibition of lysosome acidification in young testes. Using mosaic analysis, we also show that lysosomes act cell-autonomously to ensure the production of mature sperm. Collectively, these findings identify the lysosome as a critical regulator of sperm development and highlight its potential role in germline aging and infertility.

RESULTS

Lysosomes acidify in meiotic spermatocytes

To determine if lysosomes are active in male germ cells, we dissected live *Drosophila* testes and stained them with LysoTracker, a fluorescent dye that tracks to and labels acidic lysosomes. Consistent with the developmental switch in lysosome acidity that was previously reported in the *C. elegans* germline (Bohnert and Kenyon, 2017), LysoTracker staining sharply increased during germ-cell development (Figures 1B and 1C). At the apical tip, where stem cells and mitotic spermatogonia reside (Figure 1A) (de Cuevas and Matunis, 2011), LysoTracker intensity was weak (Figures 1B and 1C), with the exception of dying spermatogonia (Chiang et al., 2017; Feng et al., 2018; Lu and Yamashita, 2017; Yacobi-Sharon et al., 2013; Yang and Yamashita, 2015). However, LysoTracker intensity significantly increased in more distal regions (Figures 1B and 1C), where spermatocytes enter meiosis and differentiate (Figure 1A) (Fuller, 1998).

Previous examinations of LysoTracker staining in the apical-tip region have not reported a developmental shift in lysosome acidity (Chiang et al., 2017; Feng et al., 2018; Lu and Yamashita, 2017; Yacobi-Sharon et al., 2013; Yang and Yamashita, 2015). It is possible that dying spermatogonia, which are intensely labeled by LysoTracker (Figure S1A), obscured LysoTracker signals in neighboring healthy spermatocytes. Indeed, we consistently found that LysoTracker fluorescence needed to be overexposed in dying spermatogonia to see the underlying LysoTracker staining pattern in healthy germ cells (Figures S1A and S1B), which retained non-saturated pixels (Figures S1A and S1B). We sought to confirm the shift in lysosome acidity in healthy germ cells using two additional tools: LysoSensor Green, which fluoresces brightly in the acidic lysosomal lumen (Perzov et al., 2002), and VhaSFD-GFP, a subunit of the V-ATPase proton pump that acidifies lysosomes (Ohkuma et al., 1982). Like LysoTracker, LysoSensor signal was weak and diffuse in healthy mitotic spermatogonia, but the signal became significantly brighter and punctate in meiotic spermatocytes (Figures S1C and S1D). In addition, we found that VhaSFD-GFP protein expression abruptly increased in spermatocytes relative to spermatogonia (Figures S1E and S1F). Confirmation of the lysosome-activation pattern by these three independent tools strongly suggests that this pattern is not a staining artifact. Rather, these data collectively support the conclusion that lysosome activity is under developmental control in the male germline, increasing as germ cells move distally from the apical tip and transition from spermatogonial to spermatocyte stages.

We considered two possible explanations for the developmental shift in lysosome acidity: either (1) few lysosomes are present in the apical region of the testis, but become more abundant distally; or (2) similar numbers of lysosomes are present throughout the testis, but become active and acidic only at a certain developmental stage. To distinguish between these possibilities, we co-imaged LysoTracker with a GFP-tagged lysosomal-membrane protein, Spin-GFP (Johnson et al., 2015; Sweeney and Davis, 2002). In the mitotic region, marked by nuclei that contain a compact cloud of DNA (Figure 1A) (Cenci et al., 1994), Spin-GFP vesicles were in fact present, but lacked a co-localizing LysoTracker signal (Figures 1D and 1E). In contrast, as cells entered the meiotic region, marked by nuclei with a trilobed DNA appearance (Figure 1A) (Cenci et al., 1994), Spin-GFP vesicles developed a strong LysoTracker signal (Figures 1D, 1E, and S1B), resulting in a higher LysoTracker-to-Spin-GFP ratio (Figure 1F). Based on this information, we conclude that lysosomes acidify as germ cells enter meiosis. We confirmed this interpretation by co-imaging LysoTracker with a meiotic germ cell marker, Rbp4-eYFP (Baker et al., 2015). As expected, LysoTracker

signal was weak in regions where Rbp4-eYFP was absent, but significantly stronger where Rbp4-eYFP signal was present (Figures 1G and S1B). These data suggest that lysosomes become most highly active in meiotic germ cells.

Lysosomes regulate spermatocyte membrane integrity

To investigate the function of lysosomes in spermatocytes, we utilized an *ex vivo* tissue-culture protocol (Sheng and Matunis, 2011) to treat live *Drosophila* testes with Bafilomycin A (BafA), a lysosomal V-ATPase inhibitor (Bowman and Bowman, 2002). To affect as many cells as possible within the 80–90 h meiotic prophase (Fuller, 1998) while still keeping testes alive, we cultured dissected testes for 24 h in BafA, or in DMSO as a control. As expected, our BafA-treatment approach (Figure S2A) blocked lysosome acidification and caused lysosome enlargement (Figures S2B–S2D), perhaps because of an accumulation of non-hydrolyzed material (Leeman et al., 2018).

In contrast to the worm germline (Bohnert and Kenyon, 2017), we did not find evidence that BafA-treated testes had increased levels of insoluble proteins (Figures S2E and S2F). However, in BafA-treated testes, we frequently observed instances where a few neighboring nuclei inside of a cyst lacked a partitioning membrane and instead became encircled within a single membrane (Figures 2A and S2G). Quantification revealed that the number of germ cells missing a partitioning membrane increased significantly in BafA-treated testes relative to controls (Figure 2B). We asked whether genetic inhibition of V-ATPase activity would also engender the same phenotype. Indeed, we found that germline-specific knockdown of *vhaSFD*, which abrogated lysosome acidification (Figure 2C), recapitulated the disappearance of partitioning membranes between germ-cell nuclei (Figures 2D and 2E). Consistent with lysosome inhibition causing a defect at the meiotic stage of development, we only observed this phenotype in post-mitotic cells (Figures 2A, S2G, and S2H). We also note that it would seem unlikely for the 24-h BafA treatment to indirectly lead to this phenotype via dysfunction at a much earlier stage in development for three reasons: (1) lysosome activity is relatively low in pre-meiotic germ cells (Figure 1 and S1); (2) *Drosophila* germ cells take approximately five days in total to develop into spermatocytes after a germline stem-cell division when raised at 25°C on standard agar/cornmeal food (Fabrizio et al., 2003); and (3) we also observed loss of partitioning membranes in post-meiotic round spermatids (Figure S2H).

Because we observed some spermatocytes with odd numbers of nuclei enclosed by a common membrane (Figure S2I), we suspected that the increased absence of partitioning membranes between adjacent germ-cell nuclei may be caused by germ-cell fusion rather than cytokinesis error, as only even numbers of nuclei would be expected in the latter case (Giansanti and Fuller, 2012). A similar phenotype has been observed in old and diseased human testes (Holstein and Eckmann, 1986; Miething, 1993; Nistal et al., 1986; Paniagua et al., 1991). In these cases, plasma membranes dissolve, causing intercellular bridges to detach and become free-floating structures within the cytosol (Holstein and Eckmann, 1986). To test if this phenomenon occurs in young fly testes following inhibition of lysosome acidification, we treated testes with BafA and imaged intercellular bridges, fusomes, and rings canals. Normally, intact fusomes branch through ring canals, connecting the cytoplasm of each cell in a cyst (Figure 2F, left panel) (Giansanti et al., 1999; Hime et al., 1996). In BafA-treated testes, however, fusomes were fragmented (Figure 2F, right panel) and were commonly observed as isolated pieces within the cytosol of spermatocytes that were missing a partitioning membrane (Figure 2G). A large proportion of these germ cells likewise exhibited free-floating ring canals in the cytoplasm (Figures 2H, 2I, and S2J), suggesting that membranes between neighboring germ-cell nuclei of the same cyst had in fact become destabilized and broken down. Indeed, all nuclei that shared a common membrane were in the same cyst (Figure S2K). These findings are consistent with the model that lysosome inactivation precipitates membrane instability and cellular fusion events.

Lysosome activity counteracts Ecad accumulation, one potential contributor to germ-cell membrane instability

Proper trafficking and localization of Ecad supports membrane integrity in the female *Drosophila* germline (Kline et al., 2018; Loyer et al., 2015). Abnormal localization of Ecad has been linked to ring canal widening and collapse, suggesting that Ecad turnover may be necessary to balance forces in developing germ cells (Kline et al., 2018). To determine where Ecad is expressed and localized in the male germline, we imaged endogenously-expressed Ecad-GFP in fixed and live *Drosophila* testes. Similar to the pattern of lysosome activation (Figure 1 and S1), Ecad-GFP was mostly absent from the mitotic region, except at the hub

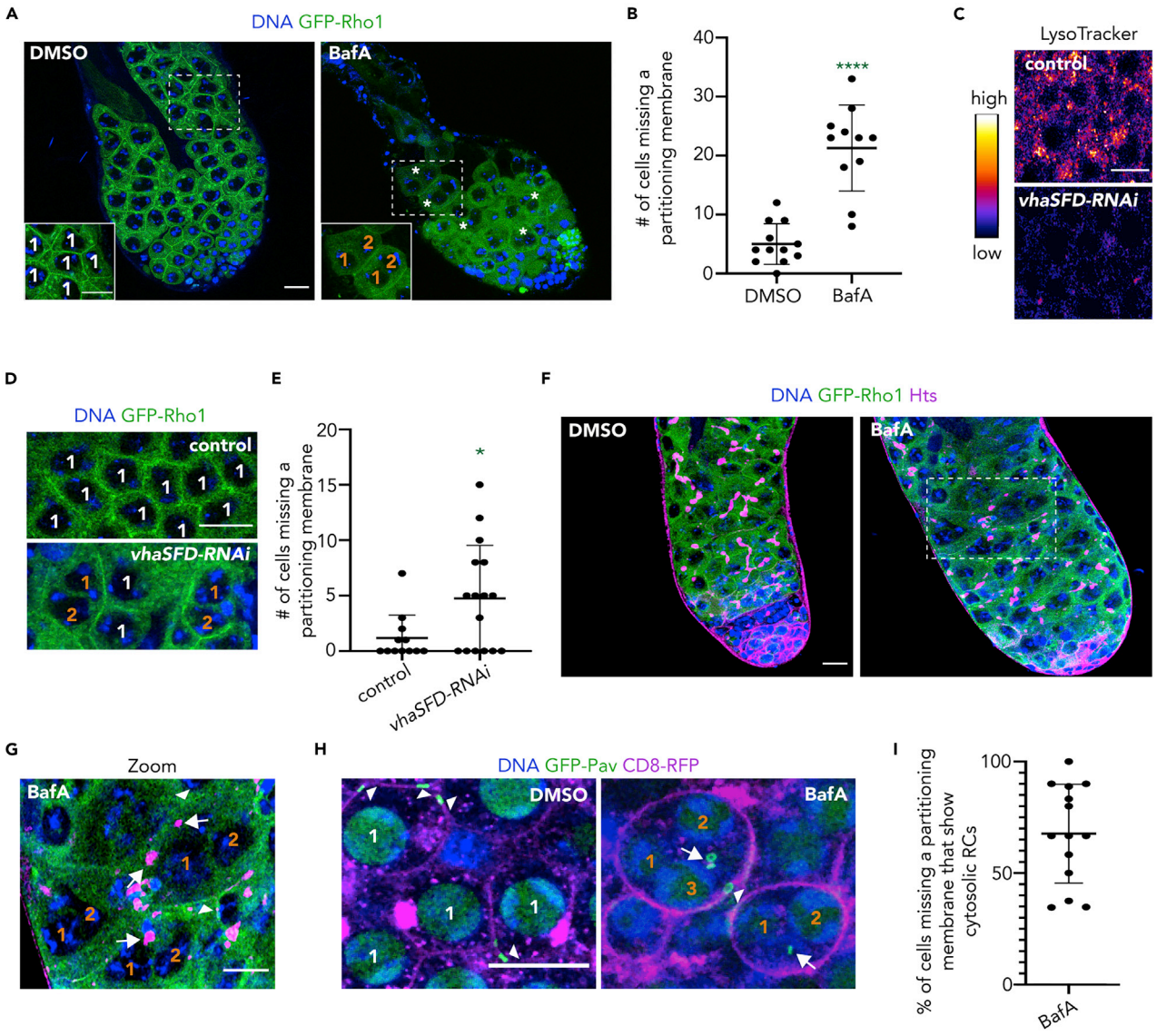

Figure 2. Inhibiting lysosome acidification causes germ-cell membrane instability in the testis

(A) Hoechst (DNA) and GFP-Rho1 (membrane marker) in live DMSO- and BafA-treated testes. Asterisks mark germ cells missing a partitioning membrane between nuclei. Dotted outlines indicate the region of the testis shown in the inset at the bottom left corner. Numbers are used to count individual nuclei enclosed within a single membrane. Orange numbering denotes groups of multiple nuclei without a partitioning membrane. These same annotations are used in all subsequent figures.

(B) Quantification of the number of germ cells missing a partitioning membrane in live DMSO- (n = 12) and BafA-treated (n = 11) testes. Mean ± S.D. ****, $p < 0.0001$, Welch's unpaired t-test.

(C) Heatmap images of LysoTracker intensity in spermatocytes of control (BamGal4/+) and *vhaSFD*-RNAi (BamGal4>*vhaSFD*-RNAi) testes.

(D) GFP-Rho1 (membrane) and Hoechst (DNA) in live control and *vhaSFD*-RNAi testes.

(E) Quantification of the number of germ cells missing a partitioning membrane in live control ($n = 12$) and *vhaSFD*-RNAi ($n = 16$) testes. Mean ± S.D. *, $p < 0.05$, Mann-Whitney U-test.

(F) Hoechst (DNA), GFP-Rho1 (membrane marker), and Hts (fusomes) in fixed DMSO- and BafA-treated testes.

(G) Zoomed image of the outlined region from the right panel of F. Arrows indicate pieces of fusomes inside the cytosol of spermatocytes missing a partitioning membrane. Arrowheads indicate membrane enclosing spermatocyte nuclei that do not have a partitioning membrane.

(H) Hoechst (DNA), GFP-Pav (ring canals), and CD8-RFP (membrane marker; driven by VasaGal4) in live DMSO- and BafA-treated testes. Arrowheads indicate ring canals that are properly localized at the cell membrane. Arrows indicate ring canals inside the cytosol of spermatocytes missing a partitioning membrane between nuclei.

(I) Quantification of the percentage of germ cells missing a partitioning membrane in BafA-treated testes that also contain at least one ring canal (RC) in their cytosol. Each data point represents a single testis ($n = 14$ testes). Bars, 20 μm. See also Figure S2.

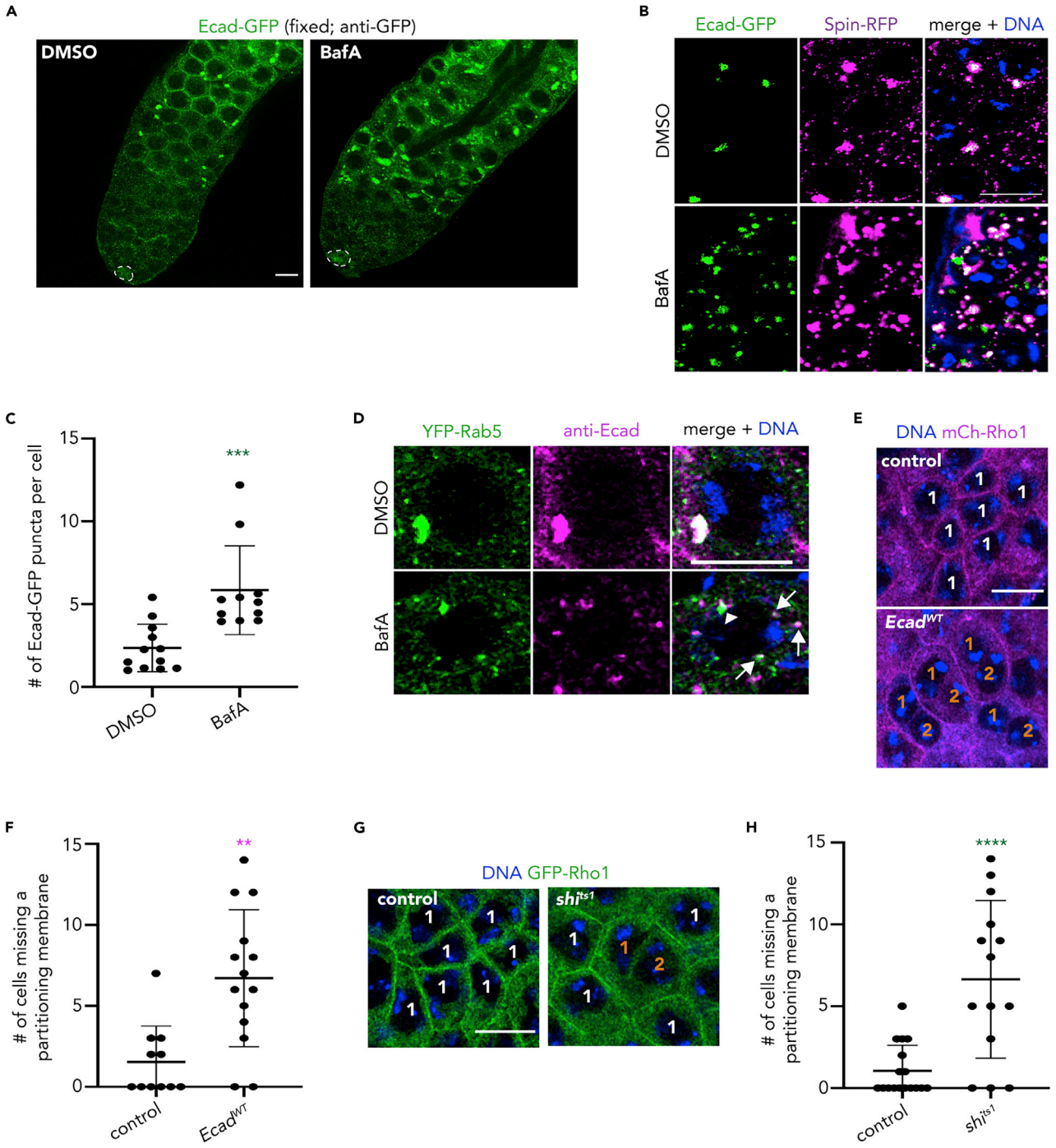

Figure 3. Endo-lysosomes concentrate around Ecad-positive hotspots and limit Ecad accumulation

(A) Ecad-GFP in fixed DMSO- or BafA-treated testes. Testes were labeled with an anti-GFP antibody. The hub (stem cell niche) is outlined.

(B) Ecad-GFP, Spin-RFP (lysosomes; driven by VasaGal4), and Hoechst (DNA) in spermatocytes (note the tri-lobed Hoechst staining pattern) of live DMSO- and BafA-treated testes.

(C) Quantification of the number of Ecad-GFP puncta per cell in live DMSO- (n = 12) and BafA-treated (n = 11) testes. Mean ± S.D. ***, $p < 0.001$, Mann-Whitney U-test.

(D) YFP-Rab5 (early endosomes; driven by VasaGal4), Ecad (anti-E-cadherin), and Hoechst (DNA) in fixed DMSO- and BafA-treated testes. The arrowhead indicates a small lysosome hotspot in the BafA-treated testis. Arrows indicate co-localization of Ecad with early endosomes apart from this hotspot.

(E) mCherry-Rho1 (membrane) and Hoechst (DNA) in live control (VasaGal4/+) and *Ecad*-overexpressing ($Ecad^{WT}$, VasaGal4>*Ecad*) testes.

Figure 3. *Continued*

(F) Quantification of the number of germ cells missing a partitioning membrane between nuclei in control (VasaGal4/+; $n = 11$) and $Ecad^{WT}$ (VasaGal4>*Ecad*; $n = 14$) testes. Mean ± S.D. ***, $p < 0.001$, Welch's unpaired t-test.

(G) GFP-Rho1 (membrane) and Hoechst (DNA) in live control (VasaGal4/+) and shi^{ts1} (VasaGal4>shi^{ts1}) testes.

(H) Quantification of the number of germ cells missing a partitioning membrane in live control (VasaGal4/+; $n = 17$) and shi^{ts1} (VasaGal4>shi^{ts1}; $n = 14$) testes. Mean ± S.D. ***, $p < 0.001$, Welch's unpaired t-test. Bars, 20 μm. See also Figure S3.

(stem cell niche) (de Cuevas and Matunis, 2011; Yamashita et al., 2003), but became more abundant as cells moved distally and began to differentiate (Figures 3A and S3A). In the meiotic region, we detected Ecad-GFP at spermatocyte cell membranes most clearly in fixed testes (Figures 3A and S3A). Yet, regardless of whether testes were imaged live or fixed, Ecad-GFP signal was especially pronounced in a few large masses (Figures 3A, 3B and S3A), which have also been detected previously (Smendziuk et al., 2015). Strikingly, these masses consistently co-localized with overlapping clusters of lysosomes and YFP-Rab5-marked endosomes (Figures S3B–S3D). In live testes, Ecad-GFP at these sites failed to recover after photobleaching, unlike cytosolic GFP (Figures S3E and S3F). Thus, Ecad is largely immobile at endo-lysosomal hotspots in developing spermatocytes.

We hypothesized that Ecad may be internalized at these sites for lysosomal degradation in developing spermatocytes. To test this possibility, we imaged Ecad-GFP after BafA treatment. Interestingly, Ecad-GFP puncta significantly accumulated following BafA treatment (Figures 3A–3C). In BafA-treated testes, some clumps of Ecad-GFP were detectable within enlarged, irregularly-shaped lysosomes, but other ectopic clumps localized separately (Figure 3B). Ectopic Ecad foci sometimes tracked closely with dispersed endosomal vesicles, which marked locations distinct from the canonical hotspots (Figure 3D). These observations suggest that lysosome inactivation may stall the proper targeting and degradation of Ecad.

Given precedence from other contexts (Kline et al., 2018; Loyer et al., 2015), we reasoned that Ecad accumulation may be one factor contributing to the observed defects in germ-cell membrane stability following V-ATPase inhibition. To test if an overabundance of Ecad can lead to membrane instability in developing spermatocytes, we overexpressed *Ecad* in the male germline and quantified the number of germ cells that were missing a partitioning membrane between adjacent nuclei. Indeed, Ecad overexpression caused a significant increase in germ cells that lacked one or more partitioning membranes (Figures 3E and 3F). We were curious whether other experimental approaches that interfered with Ecad downregulation would also be associated with this defect. Because Ecad appeared to be delivered to lysosomes via endosomes in spermatocytes (Figures 3D and S3B–S3D), we hypothesized that blocking endocytosis may impair Ecad internalization and thus its downregulation. We tested this possibility by overexpressing a temperature-sensitive, dominant-negative allele of the fly dynamin ortholog, *shibire* (shi^{ts1}) (Kitamoto, 2001; van der Bliek and Meyerowitz, 1991). Strikingly, overexpression of shi^{ts1} enhanced Ecad accumulation at spermatocyte membranes (Figure S3G) and also induced the loss of partitioning membranes (Figures 3G and 3H) to a degree similar to Ecad overexpression (Figures 3E and 3F). Notably, although genetic approaches that interfered with Ecad downregulation were sufficient to cause membrane destabilization in developing spermatocytes (Figures 3E–3H), genetic knockdown of *Ecad* in the germline (Figure S3H) was on its own insufficient to block the dissolution of partitioning membranes in BafA-treated testes (Figure S3I), indicating that deregulation of other factors also likely contributes to this phenotype upon lysosome inhibition. Thus, Ecad homeostasis may be one of several mechanisms downstream of endo-lysosomal control that govern the maintenance and stability of spermatocyte partitioning membranes during germ-cell development.

Spermatocyte lysosome activity declines during aging dependent on TOR signaling and precedes germ-cell membrane destabilization

Lysosome activity decreases with age in unicellular organisms (Hughes and Gottschling, 2012) and in somatic tissues of multicellular animals (Baxi et al., 2017). We hypothesized that lysosome activity would also decrease with age in the germline. Indeed, lysosome acidity dropped precipitously in old fly testes (Figures 4A, 4B, and S4A). Feeding flies rapamycin, a TOR inhibitor and positive regulator of lysosome activity (Martina et al., 2012; Sabatini et al., 1994), partially rescued the loss of lysosome acidity in spermatocytes from old testes (Figures 4C and 4D), suggesting that TOR signaling may negatively regulate lysosome activity in the germline, as it does in the soma (Dunlop and Tee, 2014; Martina et al., 2012; Settembre et al.,

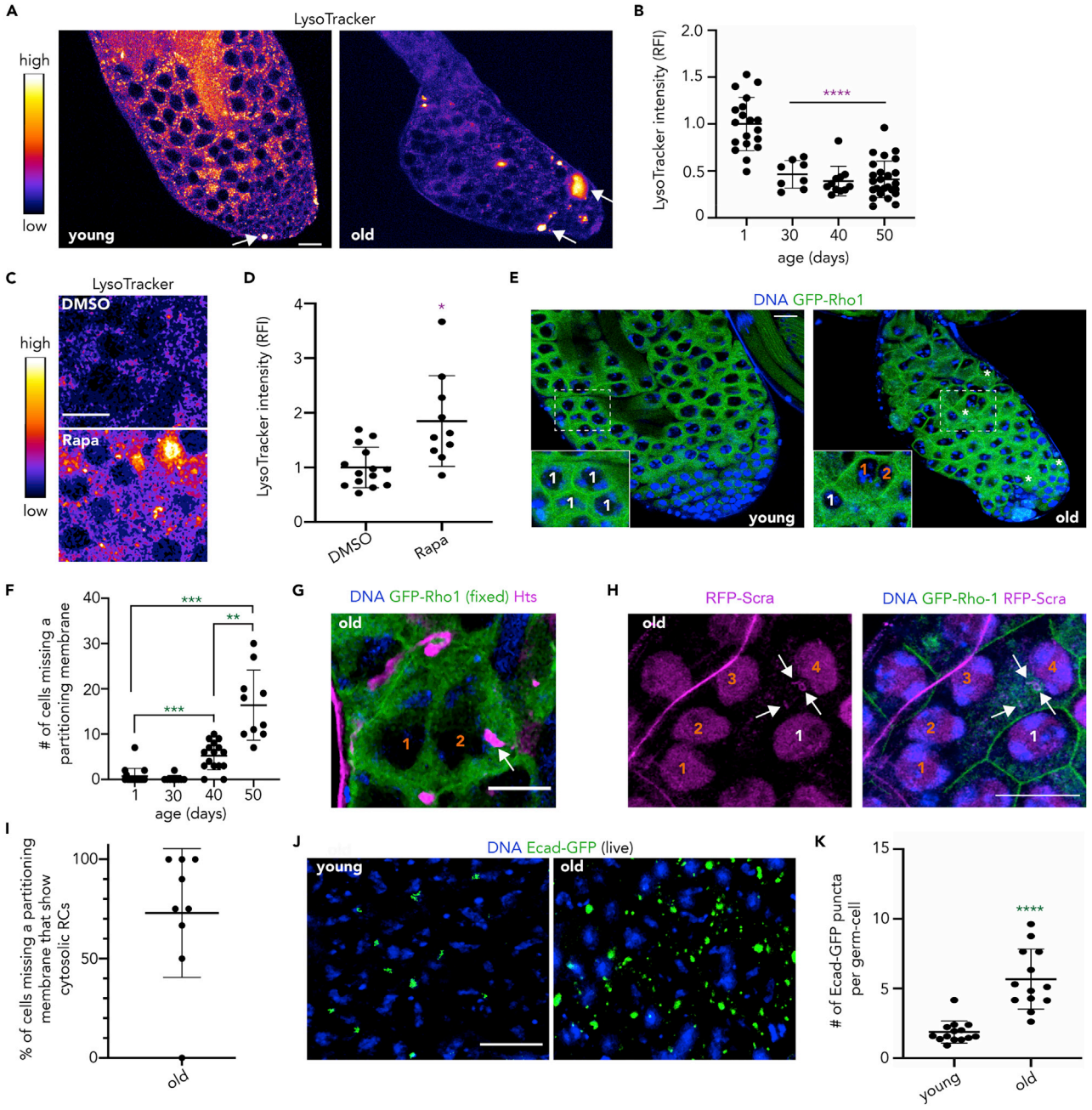

Figure 4. Aging disrupts lysosome acidification and function in the *Drosophila* testis

(A) Heatmap of LysoTracker intensity in live young (1-day-old) and old (50-day-old) testes. Arrows indicate dying spermatogonia.

(B) Quantification of LysoTracker intensity in live 1-day-old (n = 19), 30-day-old (n = 8), 40-day-old (n = 11), and 50-day-old (n = 27) testes. Mean ± S.D. ****, $p < 0.0001$, Brown-Forsythe ANOVA with Dunnett's multiple comparisons test. LysoTracker intensity in meiotic cells was normalized to dying cells.

(C) Images of LysoTracker and Hoechst (DNA) in live testes from flies fed DMSO or 10 μM rapamycin (Rapa) for four weeks beginning at day one of adulthood.

(D) Quantification of LysoTracker intensity in live testes from flies fed DMSO (control; n=14 testes) or 10 μM rapamycin (n = 10 testes) for four weeks beginning at day one of adulthood. Mean ± S.D. **, $p < 0.01$, Welch's unpaired t-test. LysoTracker intensity in meiotic cells was normalized to dying cells.

(E) Hoechst (DNA) and GFP-Rho1 (membrane marker) in live young (1-day-old) and old (50-day-old) testes. Asterisks mark spermatocytes missing a partitioning membrane between nuclei. Dotted outlines indicate the region of the testis shown in the inset at the bottom left corner.

(F) Quantification of the number of germ cells missing a partitioning membrane in live 1-day-old (n = 17), 30-day-old (n = 9), 40-day-old (n = 16), and 50-day-old (n = 10) testes. Mean ± S.D. **, $p < 0.01$; ***, $p < 0.001$, Brown-Forsythe ANOVA with Dunnett's multiple comparisons test.

(G) Hoechst (DNA), GFP-Rho1 (membrane marker), and Hts (fusomes) in spermatocytes of a fixed 50-day-old testis. The arrow indicates a piece of a fusome inside the cytosol of a spermatocyte missing a partitioning membrane between nuclei.

Figure 4. *Continued*

(H) RFP-Scra (ring canals), GFP-Rho1 (membrane marker), and Hoechst (DNA) in spermatocytes of a live 50-day-old testis. Arrows indicate ring canals inside the cytosol of a spermatocyte missing a partitioning membrane between nuclei.

(I) Quantification of the percentage of germ cells missing a partitioning membrane between nuclei in testes from old males that contain at least one ring canal (RC) in their cytosol. Each data point represents a single testis (n = 9 testes).

(J) Hoechst (DNA) and Ecad-GFP in live young (1-day-old) and old (50-day-old) testes.

(K) Quantification of the number of Ecad-GFP puncta in live young (1-day-old; n = 14) and old (50-day-old; n = 13) testes. Mean ± S.D. ****, $p < 0.0001$, Welch's unpaired t-test. Bars, 20 μm. See also Figure S4.

2012). Indeed, hyper-activation of TOR signaling via germline-specific knockdown of *iml1* (Wei et al., 2014) in young flies blocked lysosome activation and caused a significant increase in the number of germ cells missing a partitioning membrane (Figures S4B–S4E). These data indicate that germline lysosome activity is reduced with advanced age, possibly because of hyperactive TOR signaling.

We next asked whether age-related changes to lysosome acidity might naturally bring about the same cellular changes we had observed upon experimental inhibition of lysosome activity in young fly testes. In addition to lysosome enlargement (Figures S4F and S4G), we observed a progressive increase in the number of germ cells that had lost a partitioning membrane in testes from aged animals (Figures 4E and 4F). Remarkably, loss of partitioning membranes from spermatocytes in older individuals initiated just after the natural age-related decline in lysosome activity had occurred (Figures 4B and 4F). As in our BafA experiments, germ cells lacking one or more partitioning membranes commonly showed fragmented, cytosolic pieces of fusomes (Figures 4G and S4H) and on average also showed cytosolic ring canals (Figures 4H, 4I, and S4I), suggesting that the disappearance of partitioning membranes between spermatocyte nuclei may occur in old testes via membrane dissolution as it does in young, BafA-treated testes. Notably, dying spermatogonia were still present in old testes (Figure 4A, arrows); thus, the age-related accumulation of these abnormal germ cells did not appear to simply be the result of impaired spermatogonial cell death. Consistent with our BafA and genetic data, we also detected significantly more Ecad within spermatocytes of old testes compared to young testes (Figures 4J and 4K), highlighting a molecular consequence of age-related lysosome inactivity that may contribute to germ-cell membrane instability. Collectively, these data indicate that lysosomal dysfunction, which is sufficient to induce membrane destabilization (Figure 2) and naturally precedes the loss of partitioning membranes in the aging fly testis (Figures 4B and 4F), is one important element contributing to age-related membrane defects in the male germline, a characteristic of aging that is also conserved in humans (Holstein and Eckmann, 1986; Miething, 1993; Nistal et al., 1986; Paniagua et al., 1991).

Mosaic analysis reveals that lysosome activity is required cell-autonomously for the production of mature sperm

Our analyses of aging testes, as well as young testes treated with BafA or germline-specific RNAi against lysosome genes, suggested that impaired lysosome activity leads to an increase in male germ-cell defects. However, whether individual germ cells completely lacking lysosome function could ever produce a viable gamete was unclear. To test this, we utilized MARCM (Lee and Luo, 1999), a recombination-based system that bypasses lethality caused by homozygous mutations and permits the analysis of cellular effects in mosaic tissues. We generated mosaic testes containing two types of germ cells: (1) those homozygous for a null allele of the V-ATPase B subunit *vha55*; and (2) others that are wild-type at the *vha55* locus, and thus present an internal control. In the MARCM system, clones of the different genotypes can be distinguished by GFP fluorescence, as homozygous-mutant clones are GFP-labeled, whereas wild-type cells remain nonfluorescent (Figure 5A) (Lee and Luo, 1999).

In our approach, we transiently induced recombination for 1 h and then imaged testes at later time points to see if and how GFP-positive sperm developed. We first analyzed testes at 12 days post-clone induction (dpci), by which time GFP-positive cells should have neared or completed the end of sperm development if the process remained unperturbed (Chandley and Bateman, 1962). Strikingly, we never observed GFP-positive clones at 12 dpci (Figures 5B and 5C), though GFP-negative wild-type cells in the same testis developed normally and to completion, evidenced by brightly-stained, needle-shaped nuclei of elongated spermatids at the basal end of the testis (Figure 5C, outlines) and mature sperm in the seminal vesicle (Figure S5A). We confirmed that a lack of GFP-positive clones was not caused by poor recombination efficiency, or by elements of the genetic background other than the *vha55* mutation, by imaging control testes that had the same general genotype without the mutant *vha55* allele (see STAR Methods for full genotype).

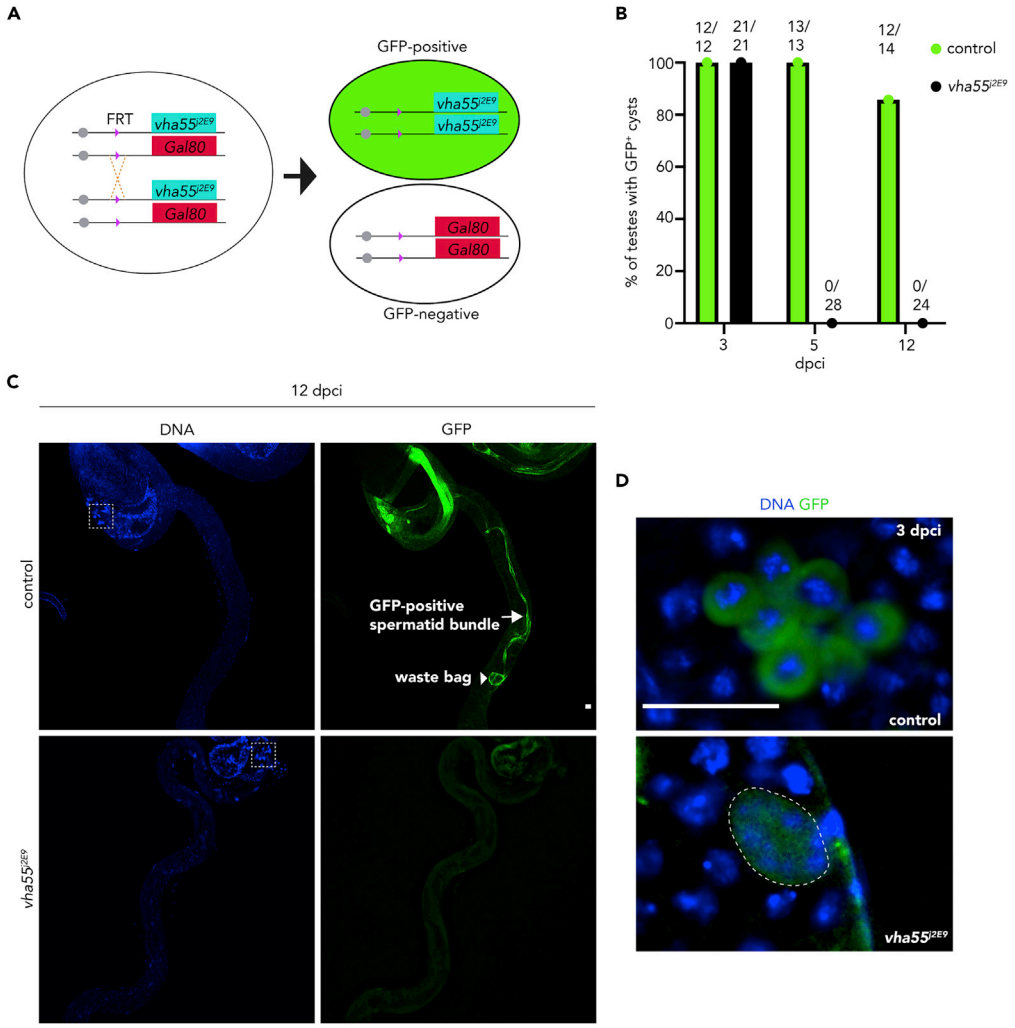

Figure 5. Lysosome activity is required cell-autonomously for germ cells to develop into mature, viable sperm

(A) Schematic of the MARCM strategy. The initial germ cell is heterozygous for a null allele of *vha55* and *Gal80*, which inhibits Gal4 activity. After heat shock ("clone induction"), recombination is induced at FRT sites (magenta arrowheads) located between Gal80 or the *vha55* locus and the centromere (gray circle). Following recombination and cell division, one cell will be homozygous for the null allele of *vha55* (*vha55*^{i2e9}), and the other cell will be homozygous for *Gal80* and homozygous wild-type at the *vha55* locus. The absence of Gal80 in *vha55*^{i2E9} homozygotes permits Gal4 activity, leading to GFP expression, whereas the other cell will express Gal80 and not GFP.

(B) Graph of the percentage of testes containing GFP-positive germ cells (MARCM clones). Numbers above each bar represent the fraction of testes containing GFP-positive germ cells.

(C) Images of Hoechst (DNA) and GFP in live control and *vha55*^{i2E9} testes at 12 dpci. Dotted outlines indicate brightly stained, needle-shaped nuclei of elongated spermatid bundles. Note the elongated spermatid bundle (arrow) and waste bag (arrowhead), an indicator of the completion of terminal differentiation, in control testes.

(D) Images of Hoechst (DNA) and GFP in live control and *vha55*^{i2E9} testes at 3 dpci. Note the healthy appearance of spermatogonia in the control image and what appears to be a smaller cyst of spermatogonia in *vha55*^{i2E9} homozygous cells (dotted outline). Bars, 20 μm. See also Figure S5.

In control testes, we consistently detected healthy GFP-positive clones (Figure 5B), including elongated spermatid bundles that had already completed the terminal differentiation step, evidenced by the presence of a waste bag (Figure 5C) (Fabian and Brill, 2012). These data suggest that mutant *vha55* homozygous germ cells are not viable and may be cleared before reaching terminal stages of sperm differentiation. Further, these data also indicate that mutant *vha55* homozygotes do not negatively affect the development of neighboring cells.

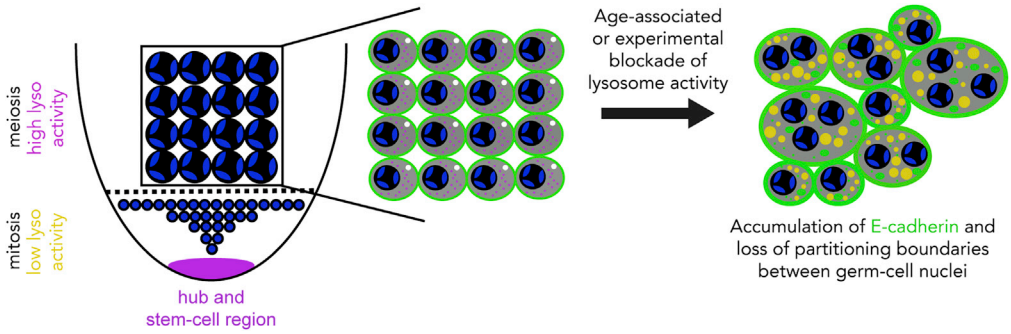

Figure 6. Model for lysosome function and dysfunction in male germ-cell development

In testes from young, healthy animals, lysosomes are mostly non-acidic and inactive in mitotic spermatogonia (solid blue nuclei), but activate (magenta circles, active lysosomes) in meiotic spermatocytes (tri-lobed nuclei). Upon this developmental transition, some lysosomes cluster with endosomes and Ecad at shared hotspots near the cell periphery (white circles). At this stage, active lysosomes limit Ecad accumulation. Lysosomal degradation of Ecad and potentially other membrane-associated factors appears to regulate membrane stability in developing spermatocytes. When lysosomes are inhibited, either experimentally via genetic or pharmacological methods or naturally during the course of aging, inactive lysosomes (yellow circles) become enlarged, Ecad accumulates (green circles), and germ cells that lack one or more partitioning membranes become prevalent.

Though we did not observe mature sperm that were homozygous for the *vha55* mutation, we were curious whether we could detect GFP-positive, *vha55*-null cells at earlier stages in sperm development. If so, we expected that we may be able to capture them before their death. Thus, we imaged mosaic testes at earlier time points post-clone induction. At 3 dpci, we were in fact able to detect GFP-positive, *vha55*-null cells in multi-cell cysts that appeared to be late-stage spermatogonia (Figures 5B and 5D). These cysts were smaller than normal and showed diffuse GFP signal (Figure 5D), in contrast to robust cytoplasmic GFP signal in germ cells of control testes (Figure 5D). Nonetheless, the presence of GFP-positive cysts at this stage indicated that *vha55*-null clones were developmentally competent of—at least—progressing through several rounds of mitotic division (Figure 1A). In contrast, at 5 dpci, by which time the developing *vha55*-null clones should have continued into meiotic prophase (Figure S5B, control) (Chandley and Bateman, 1962; Fabrizio et al., 2003), GFP-positive, *vha55*-null cells were completely undetectable (Figures 5B and S5B). This implies that *vha55*-null germ cells fail to develop through early stages of meiosis, consistent with the described important functions of lysosomes at meiotic onset during normal sperm development. Moreover, these cells appear to be ultimately cleared, as GFP-positive, *vha55*-null cells were absent from testes at both 5 and 12 dpci (Figure 5B). We conclude that inhibiting lysosome activity in individual germ-cell clones, starting from the germline stem-cell division, ultimately impedes the formation of a live, meiotic germ cell in male flies.

DISCUSSION

Although gametogenesis has been studied extensively in various experimental animals (Larose et al., 2019), there are still fundamental gaps in our knowledge of the underlying cell biology. For one, the regulation of key organelles, such as lysosomes, is somewhat mysterious. Previous work has demonstrated that lysosome activity is required for the death of mitotic spermatogonia in flies and rodents (Allan et al., 1992; Rodriguez et al., 1997; Yacobi-Sharon et al., 2013; Yang and Yamashita, 2015). Our findings highlight an additional role for lysosomes in the male germline: namely, lysosomes activate during male meiosis to support spermatocyte development and membrane integrity (Figure 6). This developmental switch in lysosome activity closely resembles the meiotic activation of lysosomes in *C. elegans* oocytes (Bohnert and Kenyon, 2017). Together, these observations indicate that a meiotic switch in lysosome activity may be conserved across species and sexes. However, the role that lysosomes play in germ cells of different sexes may be distinct. Although lysosomes appear to clear cellular damage from maturing oocytes (Bohnert and Kenyon, 2017), this function may be less important in sperm cells that contribute little cytoplasm to the zygote. Instead, lysosomes appear to execute a distinct developmental purpose in sperm, which ensures the production of a functional gamete. Interestingly, lysosome inhibition reduces the number of postmeiotic sperm cells in mice (Jaiswal et al., 2014), suggesting that lysosomes play an imperative function in the mammalian male germline as well.

More generally, developmental switches based on lysosomal activity may provide a fundamental mechanism to rewire cellular health and homeostasis at key developmental transitions. Interestingly, an analogous switch in lysosome activity was recently described during mammalian stem-cell activation (Leeman et al., 2018). In this case, lysosome activity is stimulated as neural stem cells transition from a quiescent to activated state, and lysosome activation is required for this transition. Whether conserved signals and/or factors modulate lysosome activity at these developmental transitions is unknown, but one common regulator may be TOR signaling (Leeman et al., 2018; Lu et al., 2021; Wei et al., 2014), which we have found also affects lysosome activity in the *Drosophila* male germline. Uncovering additional elements of regulation could point the way to novel applications, potentially with relevance to regenerative medicine.

The strict, invariant timing of lysosome activation as male germ cells transition from mitosis to meiosis also hints at possible controls. Spermatocytes are known to exhibit elevated gene-expression activity (Fuller, 1998), and we in fact find that the V-ATPase component VhaSFD does not accumulate in germ cells until they enter the spermatocyte stage. Thus, it seems likely that this switch in lysosome activity may be regulated in part at the level of gene expression. Mitf, the *Drosophila* ortholog of TFEB and a master regulator of lysosome biogenesis, controls the transcription of all 15 lysosomal V-ATPase components in flies (Zhang et al., 2015). Given its general role in controlling lysosomal gene expression (Settembre et al., 2011, 2012), Mitf may feed into the developmentally-linked activation of lysosomes in spermatogenesis. In future studies, it will be important to analyze how Mitf and other lysosomal factors are regulated in the germline and to determine their potential involvement in the sperm developmental program.

Once activated in the testis, lysosomes appear to govern spermatocyte membrane integrity. Of note, early endosomes and Ecad co-localize at lysosome hotspots in developing spermatocytes. This close proximity, and the increased Ecad accumulation observed upon lysosome inhibition, suggest that lysosomes target and degrade endocytosed Ecad during sperm development. Turnover of Ecad has been shown to modulate ring-canal size and membrane stability in the female *Drosophila* germline (Kline et al., 2018; Loyer et al., 2015), but the underlying mechanism by which impaired Ecad homeostasis would jeopardize membrane integrity is still unclear. It is possible that an abnormal accumulation of Ecad, and apparently even additional membrane proteins whose homeostasis is under endo-lysosomal control, may generate increased stress and tension at the membrane, leading to membrane buckling (Kline et al., 2018; Loyer et al., 2015). This could be further exacerbated by impaired plasma membrane repair, which is dependent upon lysosome activity (Castro-Gomes et al., 2016; Huynh et al., 2004). Interestingly, Ecad and other adhesion proteins are degraded by lysosomes to promote the epithelial-mesenchymal transition during cancer metastasis (Kern et al., 2015; Palacios et al., 2005; Reddy et al., 2001; Wu and Hirsch, 2009). Whether lysosomal degradation of Ecad or related proteins likewise supports germ-cell motility and migration in the testis is unknown; we do note that old testes, as well as young testes treated with BafA, often appeared wider at the apical tip and thinner in the more distal mid-region (Figures 2A, 4A, and 4E), suggesting this may be the case.

Our data highlight lysosomal dysfunction as an early cellular change that occurs naturally in the aging testis. The stepwise accumulation of atypical phenotypes with age, starting with abolished lysosome acidification and leading to the disappearance of germ-cell partitioning membranes, hints that a reduction in lysosome activity may be an initiating event in reproductive decline and infertility. If so, decreased lysosome acidity may serve as a biomarker for reproductive aging in animals. Previous reports indicate that aged testes also exhibit fewer germline stem cells (Boyle et al., 2007; Cheng et al., 2008). Although this may contribute to a reduction in total germ-cell number, it does not explain why the germ cells produced in older animals would be less capable of maturing into functional sperm. Our data indicate that lysosomes play an essential role in germ-cell viability and development beyond the stem-cell stage. Inhibition of lysosomal activity in young flies via BafA, RNAi, and MARCM yielded a series of phenotypes that varied in severity, likely because of differences in the strength of inhibition (RNAi vs. null mutant) as well as the timing and duration of inhibition (24 h BafA treatment vs. 3–12 days after clone induction for MARCM experiments). Although we were unable to determine the ultimate fate of germ cells that had lost partitioning membranes upon BafA treatment, it seems likely that these cells would be incompetent to produce viable progeny given their extra chromosomal content, and they may even eventually be cleared from the reproductive tissue. Indeed, using MARCM, we found that *vha55*-null germ cells do not persist through the spermatocyte stage, perhaps because of the cumulative effect of several deleterious phenotypes, including membrane destabilization. Taken together, our findings suggest that deregulation of later events in spermatogenesis, such

as lysosome induction, may act along with stem-cell dysfunction to synergistically limit the output of functional sperm in older males.

Finally, it is noteworthy that a defining characteristic of male germline aging in humans is germ-cell multinucleation (Holstein and Eckmann, 1986; Miething, 1993). Because we find that dissolution of germ-cell boundaries occurs upon the loss of lysosome activity in male flies, it is possible that targeted activation of lysosomal factors may act to enhance gamete viability and reproductive fitness in animals, similar to its effects on replicative potential in single-celled yeast (Hughes and Gottschling, 2012). Thus, we speculate that lysosomes may provide an entry point to target, and potentially counter, male reproductive aging in animal species.

Limitations of the study

Our data indicate that lysosomes prevent the breakdown of partitioning membranes between post-mitotic germ-cell nuclei during spermatogenesis, and that lysosome acidity is reduced around the time of male fly infertility. Strikingly, we found that inhibiting TOR signaling via rapamycin feeding throughout adulthood prevented this loss of germline lysosome acidity at four-weeks of age, when male flies typically exhibited reduced lysosome acidity. Ideally, we would like to analyze whether this is sufficient to counter the accumulation of germ cells missing a partitioning membrane. However, spermatogonial cell number also greatly increased in testes from males that were fed rapamycin, and these testes contained fewer spermatocytes compared to controls. Though we noted fewer spermatocytes missing a partitioning membrane in testes from males fed rapamycin, it is hard to discern whether this reduction is because of rapamycin feeding or instead simply because of there being fewer spermatocytes. Because of this apparent secondary effect, we were unable to confidently assess whether rapamycin feeding would also suppress germ-cell membrane instability in old testes. Relatedly, it would be experimentally powerful if we could genetically knockdown TOR signaling components specifically in spermatocytes to test for a suppression of age-related germ-cell membrane instability. Unfortunately, to our knowledge, a Gal4 driver that is specifically active in spermatocytes does not currently exist. Going forward, it will be important to generate flies carrying a Gal4 transgene under control of a promoter that is specifically active in spermatocytes to determine whether TOR inhibition in spermatocytes dampens the age-associated loss of partitioning membranes between developing male germ cells.

Lastly, we were unable to definitively determine the ultimate fate of germ cells that lose partitioning membranes upon BafA or lysosome-specific RNAi treatment. In later stages of development, following spermatid elongation, nuclei are very close together, making it difficult to resolve membranes between nuclei. In the future, imaging techniques that permit higher resolution, such as super resolution and/or electron microscopy, may be employed to determine whether elongated spermatids or mature sperm containing multiple nuclei can form and survive under these conditions, or if they are potentially eliminated before this developmental time point, as appears to be the case for *vha55*-null cells.

STAR★METHODS

Detailed methods are provided in the online version of this paper and include the following:

- KEY RESOURCES TABLE
- RESOURCE AVAILABILITY
  - Lead contact
  - Materials availability
  - Data and code availability
- EXPERIMENTAL MODEL AND SUBJECT DETAILS
- METHOD DETAILS
  - BafA treatment
  - Immunohistochemistry
  - LysoTracker, LysoSensor, and ProteoStat staining
  - Microscopy and image processing
  - Lysosomal area measurement
  - Quantification of germ cells missing a partitioning membrane
  - FRAP experiments
  - Aging studies

- Rapamycin feeding
- RNAi and mutant experiments
- MARCM
- Insoluble-protein fractionation

- QUANTIFICATION AND STATISTICAL ANALYSIS

SUPPLEMENTAL INFORMATION

Supplemental information can be found online at https://doi.org/10.1016/j.isci.2022.104382.

ACKNOWLEDGMENTS

This work was supported by the LSU Office of Research & Economic Development, the LSU College of Science, and the LSU Department of Biological Science (A.E.J. and K.A.B.); National Institutes of Health grants R00NS100988 and R35GM138116 (A.E.J.); and the LSU Ron and Mary Neal Distinguished Graduate Student Fellowship (T.J.B). The LSU Department of Biological Sciences subsidized use of the Leica SP8 confocal microscope in the LSU Shared Instrumentation Facility. We thank Margaret Fuller (Stanford University), Leanne Jones (UCSF), Mary Lilly (NIH), Doug Harrison (UK), SeYeon Chung (LSU), the Bloomington *Drosophila* Stock Center, and the Developmental Studies Hybridoma Bank for providing fly stocks and antibodies. We also thank members of the Bohnert and Johnson labs for helpful discussions and critical reading of this manuscript.

AUTHOR CONTRIBUTIONS

Conceptualization, T.J.B. and K.A.B.; Methodology, T.J.B., O.D., A.E.J., and K.A.B.; Investigation, T.J.B.; Writing, T.J.B. and K.A.B.; Funding Acquisition, T.J.B., A.E.J., and K.A.B.; Resources, T.J.B., O.D., A.E.J., and K.A.B.; Supervision, A.E.J. and K.A.B.

DECLARATION OF INTERESTS

The authors declare no competing interests.

Received: September 11, 2021
Revised: December 1, 2021
Accepted: May 5, 2022
Published: June 17, 2022

REFERENCES

Allan, D.J., Harmon, B.V., and Roberts, S.A. (1992). Spermatogonial apoptosis has three morphologically recognizable phases and shows no circadian rhythm during normal spermatogenesis in the rat. Cell Prolif. *25*, 241–250. https://doi.org/10.1111/j.1365-2184.1992.tb01399.x.

Baker, C.C., Gim, B.S., and Fuller, M.T. (2015). Cell type-specific translational repression of Cyclin B during meiosis in males. Development *142*, 3394–3402. https://doi.org/10.1242/dev.122341.

Ballabio, A., and Bonifacino, J.S. (2020). Lysosomes as dynamic regulators of cell and organismal homeostasis. Nat. Rev. Mol. Cell Biol. *21*, 101–118. https://doi.org/10.1038/s41580-019-0185-4.

Baxi, K., Ghavidel, A., Waddell, B., Harkness, T.A., and de Carvalho, C.E. (2017). Regulation of lysosomal function by the DAF-16 forkhead transcription factor couples reproduction to aging in Caenorhabditis elegans. Genetics *207*, 83–101. https://doi.org/10.1534/genetics.117.204222.

Bohnert, K.A., and Kenyon, C. (2017). A lysosomal switch triggers proteostasis renewal in the immortal C. elegans germ lineage. Nature *551*, 629–633. https://doi.org/10.1038/nature24620.

Bowman, B.J., and Bowman, E.J. (2002). Mutations in subunit c of the vacuolar ATPase confer resistance to Bafilomycin and identify a conserved antibiotic binding site. J. Biol. Chem. *277*, 3965–3972. https://doi.org/10.1074/jbc.M109756200.

Boyle, M., Wong, C., Rocha, M., and Jones, D.L. (2007). Decline in self-renewal factors contributes to aging of the stem cell niche in the Drosophila testis. Cell Stem Cell *1*, 470–478. https://doi.org/10.1016/j.stem.2007.08.002.

Castro-Gomes, T., Corrotte, M., Tam, C., and Andrews, N.W. (2016). Plasma membrane repair is regulated extracellularly by proteases released from lysosomes. PLoS One *11*, e0152583. https://doi.org/10.1371/journal.pone.0152583.

Cenci, G., Bonaccorsi, S., Pisano, C., Verni, F., and Gatti, M. (1994). Chromatin and microtubule organization during premeiotic, meiotic and early postmeiotic stages of Drosophila melanogaster spermatogenesis. J. Cell Sci. *107*, 3521–3534. https://doi.org/10.1242/jcs.107.12.3521.

Chandley, A.C., and Bateman, A.J. (1962). Timing of spermatogenesis in Drosophila melanogaster using tritiated thymidine. Nature *193*, 299–300. https://doi.org/10.1038/193299b0.

Chen, D., and McKearin, D.M. (2003). A discrete transcriptional silencer in the bam gene determines asymmetric division of the Drosophila germline stem cell. Development *130*, 1159–1170. https://doi.org/10.1242/dev.00325.

Cheng, J., Türkel, N., Hemati, N., Fuller, M.T., Hunt, A.J., and Yamashita, Y.M. (2008). Centrosome misorientation reduces stem cell division during ageing. Nature *456*, 599–604. https://doi.org/10.1038/nature07386. https://www.nature.com/articles/nature07386#supplementary-information.

Chiang, A.C.Y., Yang, H., and Yamashita, Y.M. (2017). spict, a cyst cell-specific gene, regulates starvation-induced spermatogonial cell death in the Drosophila testis. Sci. Rep. *7*, 40245. https://doi.org/10.1038/srep40245. https://www.nature.com/articles/srep40245#supplementary-information.

de Cuevas, M., and Matunis, E.L. (2011). The stem cell niche: lessons from the Drosophila testis.

Development *138*, 2861–2869. https://doi.org/10.1242/dev.056242.

Dunlop, E.A., and Tee, A.R. (2014). mTOR and autophagy: a dynamic relationship governed by nutrients and energy. Semin. Cell Dev. Biol. *36*, 121–129. https://doi.org/10.1016/j.semcdb.2014.08.006.

Fabian, L., and Brill, J.A. (2012). Drosophila spermiogenesis: big things come from little packages. Spermatogenesis *2*, 197–212. https://doi.org/10.4161/spmg.21798.

Fabrizio, J.J., Boyle, M., and DiNardo, S. (2003). A somatic role for eyes absent (eya) and sine oculis (so) in drosophila spermatocyte development. Dev. Biol. *258*, 117–128. https://doi.org/10.1016/S0012-1606(03)00127-1.

Feng, L., Shi, Z., Xie, J., Ma, B., and Chen, X. (2018). Enhancer of polycomb maintains germline activity and genome integrity in Drosophila testis. Cell Death Differ. *25*, 1486–1502. https://doi.org/10.1038/s41418-017-0056-5.

Fuller, M.T. (1993). Spermatogenesis. In The Development of Drosophila melanogaster, M. Bate and A. Martinez Arias, eds. (Cold Spring Harbor Laboratory Press), pp. 71–147.

Fuller, M.T. (1998). Genetic control of cell proliferation and differentiation in Drosophila spermatogenesis. Semin. Cell Dev. Biol. *9*, 433–444. https://doi.org/10.1006/scdb.1998.0227.

Giansanti, M.G., Bonaccorsi, S., and Gatti, M. (1999). The role of anillin in meiotic cytokinesis of Drosophila males. J. Cell Sci. *112*, 2323–2334. https://doi.org/10.1242/jcs.112.14.2323.

Giansanti, M.G., and Fuller, M.T. (2012). What Drosophila spermatocytes tell us about the mechanisms underlying cytokinesis. Cytoskeleton (Hoboken, N.J.) *69*, 869–881. https://doi.org/10.1002/cm.21063.

Griswold, M.D. (2016). Spermatogenesis: the commitment to meiosis. Physiol. Rev. *96*, 1–17. https://doi.org/10.1152/physrev.00013.2015.

Harris, I.D., Fronczak, C., Roth, L., and Meacham, R.B. (2011). Fertility and the aging male. Rev. Urol. *13*, e184–e190.

Hennig, W. (1992). Drosophila spermatogenesis as a model system. Andrologia *24*, 21–26. https://doi.org/10.1111/j.1439-0272.1992.tb02603.x.

Hime, G.R., Brill, J.A., and Fuller, M.T. (1996). Assembly of ring canals in the male germ line from structural components of the contractile ring. J. Cell Sci. *109*, 2779–2788. https://doi.org/10.1242/jcs.109.12.2779.

Holstein, A.F., and Eckmann, C. (1986). Multinucleated spermatocytes and spermatids in human seminiferous tubules. Andrologia *18*, 5–16. https://doi.org/10.1111/j.1439-0272.1986.tb01729.x.

Hughes, A.L., and Gottschling, D.E. (2012). An early age increase in vacuolar pH limits mitochondrial function and lifespan in yeast. Nature *492*, 261–265. https://doi.org/10.1038/nature11654. https://www.nature.com/articles/nature11654#supplementary-information.

Huynh, C., Roth, D., Ward, D.M., Kaplan, J., and Andrews, N.W. (2004). Defective lysosomal exocytosis and plasma membrane repair in Chediak–Higashi/beige cells. Proc. Natl. Acad. Sci. U S A *101*, 16795–16800. https://doi.org/10.1073/pnas.0405905101.

Jaiswal, M.K., Katara, G.K., Mallers, T., Chaouat, G., Gilman-Sachs, A., and Beaman, K.D. (2014). Vacuolar-ATPase isoform a2 regulates macrophages and cytokine profile necessary for normal spermatogenesis in testis. J. Leukoc. Biol. *96*, 337–347. https://doi.org/10.1189/jlb.3A1113-593RR.

Johnson, A.E., Shu, H., Hauswirth, A.G., Tong, A., and Davis, G.W. (2015). VCP-dependent muscle degeneration is linked to defects in a dynamic tubular lysosomal network in vivo. Elife *4*, e07366. https://doi.org/10.7554/eLife.07366.

Kern, U., Wischnewski, V., Biniossek, M.L., Schilling, O., and Reinheckel, T. (2015). Lysosomal protein turnover contributes to the acquisition of TGFβ-1 induced invasive properties of mammary cancer cells. Mol. Cancer *14*, 39. https://doi.org/10.1186/s12943-015-0313-5.

Kitamoto, T. (2001). Conditional modification of behavior in Drosophila by targeted expression of a temperature-sensitive shibire allele in defined neurons. J. Neurobiol. *47*, 81–92. https://doi.org/10.1002/neu.1018.

Kline, A., Curry, T., and Lewellyn, L. (2018). The Misshapen kinase regulates the size and stability of the germline ring canals in the Drosophila egg chamber. Dev. Biol. *440*, 99–112. https://doi.org/10.1016/j.ydbio.2018.05.006.

Kumar, N., and Singh, A.K. (2015). Trends of male factor infertility, an important cause of infertility: a review of literature. J. Hum. Reprod. Sci. *8*, 191–196. https://doi.org/10.4103/0974-1208.170370.

Larose, H., Shami, A.N., Abbott, H., Manske, G., Lei, L., and Hammoud, S.S. (2019). Gametogenesis: a journey from inception to conception. Curr. Top. Dev. Biol. *132*, 257–310. https://doi.org/10.1016/bs.ctdb.2018.12.006.

Lee, T., and Luo, L. (1999). Mosaic analysis with a repressible cell marker for studies of gene function in neuronal morphogenesis. Neuron *22*, 451–461. https://doi.org/10.1016/S0896-6273(00)80701-1.

Leeman, D.S., Hebestreit, K., Ruetz, T., Webb, A.E., McKay, A., Pollina, E.A., Dulken, B.W., Zhao, X., Yeo, R.W., Ho, T.T., et al. (2018). Lysosome activation clears aggregates and enhances quiescent neural stem cell activation during aging. Science *359*, 1277–1283. https://doi.org/10.1126/science.aag3048.

Lin, T.Y., Viswanathan, S., Wood, C., Wilson, P.G., Wolf, N., and Fuller, M.T. (1996). Coordinate developmental control of the meiotic cell cycle and spermatid differentiation in Drosophila males. Development *122*, 1331–1341. https://doi.org/10.1242/dev.122.4.1331.

Loyer, N., Kolotuev, I., Pinot, M., and Le Borgne, R. (2015). Drosophila E-cadherin is required for the maintenance of ring canals anchoring to mechanically withstand tissue growth. Proc. Natl. Acad. Sci. U S A *112*, 12717–12722. https://doi.org/10.1073/pnas.1504455112.

Lu, K.L., and Yamashita, Y.M. (2017). Germ cell connectivity enhances cell death in response to DNA damage in the Drosophila testis. Elife *6*, e27960. https://doi.org/10.7554/eLife.27960.

Lu, Y.-X., Regan, J.C., Eßer, J., Drews, L.F., Weinseis, T., Stinn, J., Hahn, O., Miller, R.A., Grönke, S., and Partridge, L. (2021). A TORC1-histone axis regulates chromatin organisation and non-canonical induction of autophagy to ameliorate ageing. Elife *10*, e62233. https://doi.org/10.7554/eLife.62233.

Martina, J.A., Chen, Y., Gucek, M., and Puertollano, R. (2012). MTORC1 functions as a transcriptional regulator of autophagy by preventing nuclear transport of TFEB. Autophagy *8*, 903–914. https://doi.org/10.4161/auto.19653.

Meyer, J.M., Maetz, J.L., and Rumpler, Y. (1992). Cellular relationship impairment in maturation arrest of human spermatogenesis: an ultrastructural study. Histopathology *21*, 25–33. https://doi.org/10.1111/j.1365-2559.1992.tb00339.x.

Miething, A. (1993). Multinucleated spermatocytes in the aging human testis: formation, morphology, and degenerative fate. Andrologia *25*, 317–323. https://doi.org/10.1111/j.1439-0272.1993.tb02733.x.

Nistal, M., Codesal, J., and Paniagua, R. (1986). Multinucleate spermatids in aging human testes. Arch. Androl. *16*, 125–129. https://doi.org/10.3109/01485018608986931.

Ohkuma, S., Moriyama, Y., and Takano, T. (1982). Identification and characterization of a proton pump on lysosomes by fluorescein-isothiocyanate-dextran fluorescence. Proc. Natl. Acad. Sci. U S A *79*, 2758–2762. https://doi.org/10.1073/pnas.79.9.2758.

Palacios, F., Tushir, J.S., Fujita, Y., and D'Souza-Schorey, C. (2005). Lysosomal targeting of E-cadherin: a unique mechanism for the down-regulation of cell-cell adhesion during epithelial to mesenchymal transitions. Mol. Cell. Biol. *25*, 389–402. https://doi.org/10.1128/MCB.25.1.389-402.2005.

Paniagua, R., Nistal, M., Sáez, F.J., and Fraile, B. (1991). Ultrastructure of the aging human testis. J. Electron Microsc. Tech. *19*, 241–260. https://doi.org/10.1002/jemt.1060190209.

Perzov, N., Padler-Karavani, V., Nelson, H., and Nelson, N. (2002). Characterization of yeast V-ATPase mutants lacking Vph1p or Stv1p and the effect on endocytosis. J. Exp. Biol. *205*, 1209–1219. https://doi.org/10.1242/jeb.205.9.1209.

Reddy, A., Caler, E.V., and Andrews, N.W. (2001). Plasma membrane repair is mediated by Ca2+ regulated exocytosis of lysosomes. Cell *106*, 157–169. https://doi.org/10.1016/S0092-8674(01)00421-4.

Rodriguez, I., Ody, C., Araki, K., Garcia, I., and Vassalli, P. (1997). An early and massive wave of germinal cell apoptosis is required for the development of functional spermatogenesis. EMBO J. *16*, 2262–2270. https://doi.org/10.1093/emboj/16.9.2262.

Ruman, J., Klein, J., and Sauer, M.V. (2003). Understanding the effects of age on female fertility. Minerva Ginecol. *55*, 117–127.

Sabatini, D.M., Erdjument-Bromage, H., Lui, M., Tempst, P., and Snyder, S.H. (1994). RAFT1: a mammalian protein that binds to FKBP12 in a rapamycin-dependent fashion and is homologous to yeast TORs. Cell *78*, 35–43. https://doi.org/10.1016/0092-8674(94)90570-3.

Schinaman, J.M., Rana, A., Ja, W.W., Clark, R.I., and Walker, D.W. (2019). Rapamycin modulates tissue aging and lifespan independently of the gut microbiota in Drosophila. Sci. Rep. *9*, 7824. https://doi.org/10.1038/s41598-019-44106-5.

Settembre, C., Di Malta, C., Polito, V.A., Arencibia, M.G., Vetrini, F., Erdin, S., Erdin, S.U., Huynh, T., Medina, D., Colella, P., et al. (2011). TFEB links autophagy to lysosomal biogenesis. Science *332*, 1429–1433. https://doi.org/10.1126/science.1204592.

Settembre, C., Zoncu, R., Medina, D.L., Vetrini, F., Erdin, S., Erdin, S., Huynh, T., Ferron, M., Karsenty, G., Vellard, M.C., et al. (2012). A lysosome-to-nucleus signalling mechanism senses and regulates the lysosome via mTOR and TFEB. EMBO J. *31*, 1095–1108. https://doi.org/10.1038/emboj.2012.32.

Sheng, X.R., and Matunis, E. (2011). Live imaging of the Drosophila spermatogonial stem cell niche reveals novel mechanisms regulating germline stem cell output. Development *138*, 3367–3376. https://doi.org/10.1242/dev.065797.

Smendziuk, C.M., Messenberg, A., Vogl, W., and Tanentzapf, G. (2015). Bi-directional gap junction-mediated soma-germline communication is essential for spermatogenesis. Development *142*, 2598. https://doi.org/10.1242/dev.123448.

Soderstrom, K.O., and Suominen, J. (1980). Histopathology and ultrastructure of meiotic arrest in human spermatogenesis. Arch. Pathol. Lab. Med. *104*, 476–482.

Sweeney, S.T., and Davis, G.W. (2002). Unrestricted synaptic growth in spinster a late endosomal protein implicated in TGF-beta-mediated synaptic growth regulation. Neuron *36*, 403–416. https://doi.org/10.1016/S0896-6273(02)01014-0.

van der Bliek, A.M., and Meyerowrtz, E.M. (1991). Dynamin-like protein encoded by the Drosophila shibire gene associated with vesicular traffic. Nature *351*, 411–414. https://doi.org/10.1038/351411a0.

Villegas, F., Lehalle, D., Mayer, D., Rittirsch, M., Stadler, M.B., Zinner, M., Olivieri, D., Vabres, P., Duplomb-Jego, L., De Bont, E.S.J.M., et al. (2019). Lysosomal signaling licenses embryonic stem cell differentiation via inactivation of Tfe3. Cell Stem Cell *24*, 257–270.e8. https://doi.org/10.1016/j.stem.2018.11.021.

Wei, Y., Reveal, B., Reich, J., Laursen, W.J., Senger, S., Akbar, T., Iida-Jones, T., Cai, W., Jarnik, M., and Lilly, M.A. (2014). TORC1 regulators Iml1/GATOR1 and GATOR2 control meiotic entry and oocyte development in Drosophila. Proc. Natl. Acad. Sci. U S A *111*, E5670. https://doi.org/10.1073/pnas.1419156112.

White-Cooper, H., Schafer, M.A., Alphey, L.S., and Fuller, M.T. (1998). Transcriptional and post-transcriptional control mechanisms coordinate the onset of spermatid differentiation with meiosis I in Drosophila. Development *125*, 125–134. https://doi.org/10.1242/dev.125.1.125.

Wu, W.J., and Hirsch, D.S. (2009). Mechanism of E-cadherin lysosomal degradation. Nat. Rev. Cancer *9*, 143. https://doi.org/10.1038/nrc2521-c1.

Xie, S.Z., Garcia-Prat, L., Voisin, V., Ferrari, R., Gan, O.I., Wagenblast, E., Kaufmann, K.B., Zeng, A.G.X., Takayanagi, S.-i., Patel, I., et al. (2019). Sphingolipid modulation activates proteostasis programs to govern human hematopoietic stem cell self-renewal. Cell Stem Cell *25*, 639–653.e7. https://doi.org/10.1016/j.stem.2019.09.008.

Yacobi-Sharon, K., Namdar, Y., and Arama, E. (2013). Alternative germ cell death pathway in Drosophila involves HtrA2/Omi, lysosomes, and a caspase-9 counterpart. Dev. Cell *25*, 29–42. https://doi.org/10.1016/j.devcel.2013.02.002.

Yamashita, Y.M., Jones, D.L., and Fuller, M.T. (2003). Orientation of asymmetric stem cell division by the APC tumor suppressor and centrosome. Science *301*, 1547–1550. https://doi.org/10.1126/science.1087795.

Yang, H., and Yamashita, Y.M. (2015). The regulated elimination of transit-amplifying cells preserves tissue homeostasis during protein starvation in Drosophila testis. Development *142*, 1756–1766. https://doi.org/10.1242/dev.122663.

Zhang, T., Zhou, Q., Ogmundsdottir, M.H., Möller, K., Siddaway, R., Larue, L., Hsing, M., Kong, S.W., Goding, C.R., Palsson, A., et al. (2015). Mitf is a master regulator of the v-ATPase forming an Mitf/v-ATPase/TORC1 control module for cellular homeostasis. J. Cell Sci. *128*, 2938–2950. https://doi.org/10.1242/jcs.173807.

Zhao, S., Chen, D., Geng, Q., and Wang, Z. (2013). The highly conserved LAMMER/CLK2 protein kinases prevent germ cell overproliferation in Drosophila. Dev. Biol. *376*, 163–170. https://doi.org/10.1016/j.ydbio.2013.01.023.

STAR★METHODS

KEY RESOURCES TABLE

REAGENT or RESOURCE	SOURCE	IDENTIFIER
Antibodies		
Rabbit anti-GFP	Invitrogen	RRID: AB_221477 Cat# A21311
Mouse anti-Hts	DSHB (H.D. Lipshitz)	RRID: AB_528070 1B1
Rat anti-E-cadherin	DSHB (T. Uemura)	RRID: AB_528120 DCAD2
Mouse anti-Arm	DSHB (E. Wieschaus)	RRID: AB_528089 N2 7A1
Goat anti-rabbit 488	Invitrogen	RRID: AB_2576217 Cat# A11034
Goat anti-mouse 555	Invitrogen	RRID: AB_141822 Cat# A21422
Goat anti-rat 568	Invitrogen	RRID: AB_141874 Cat# A11077
Chemicals, peptides, and recombinant proteins		
Bafilomycin A1	Sigma	Cat #B1793
Rapamycin	LC Laboratories	Cat# R-5000
LysoTracker Red DND-99	Invitrogen	Cat# L7528
LysoSensor Green DND-189	Invitrogen	Cat# L7535
Hoechst 33342	Invitrogen	Cat# H21492
ProteoStat	Enzo Life Sciences	Cat# ENZ-51035-0025
Antifade mounting medium	Vectashield	Cat# H1000
NuPAGE 4-12% Bis Tris Gel	Invitrogen	Cat# NP0322BOX
Coomassie blue	Biorad	Cat #1610786
Experimental models: Organisms/strains		
D. melanogaster: Rbp4-eYFP	Laboratory of M. Fuller (Stanford)	N/A
D. melanogaster: VasaGal4	Laboratory of L. Jones (UCSF)	N/A
D. melanogaster: Ecad-GFP	Laboratory of S. Chung (LSU)	N/A
D. melanogaster: UAS-*iml1*-RNAi	Laboratory of M. Lilly (NIH)	N/A
D. melanogaster: BamGal4	Laboratory of D. Harrison (U. Kentucky)	N/A
D. melanogaster: hsFLP.D5, UAS-GFP	Bloomington *Drosophila* Stock Center (BDSC)	90894
D. melanogaster: UAS-Ecad-GFP	BDSC	58445
D. melanogaster: FRT82B, tubGal80	BDSC	5135
D. melanogaster: FRT82B	BDSC	86313
D. melanogaster: UAS-*vhaSFD*-RNAi	BDSC	40896
D. melanogaster: VhaSFD-GFP	BDSC	6840
D. melanogaster: UAS-Spin-GFP	BDSC	39668
D. melanogaster: UAS-Spin-RFP	BDSC	42716
D. melanogaster: GFP-Rho1	BDSC	9528
D. melanogaster: mCherry-Rho1	BDSC	52281
D. melanogaster: GFP-Pav	BDSC	81651
D. melanogaster: UAS-RFP-Scra	BDSC	52220

(*Continued on next page*)

Continued

REAGENT or RESOURCE	SOURCE	IDENTIFIER
D. melanogaster: UAS-YFP-Rab5	BDSC	24616
D. melanogaster: vha55^{i2E9}	BDSC	12128
D. melanogaster: UAS-*Ecad*-RNAi	BDSC	32904
D. melanogaster: UAS-*shi*^{ts1}	BDSC	44222
D. melanogaster: UAS-CD8-GFP	Lab stock	N/A
D. melanogaster: UAS-CD8-RFP	Lab stock	N/A
Software and algorithms		
ImageJ v2.3	Wayne Rasband, NIH	https://imagej.nih.gov/ij
Illustrator CC 2020	Adobe	N/A
Prism v8.4	Graphpad	N/A
Other		
Schneider's insect medium	Gibco/Invitrogen	Cat# 11720034
Fetal Bovine Serum	Sigma	Cat# F3018
Penicillin/Streptomycin	Gibco/Invitrogen	Cat# 115140-122
Bovine insulin	Sigma	Cat# I550
Teflon membrane	YSI Life Science	Cat #5793

RESOURCE AVAILABILITY

Lead contact

Further information and requests for reagents should be directed to and will be fulfilled by the lead contact, K. Adam Bohnert (bohnerta@lsu.edu).

Materials availability

All unique materials and reagents generated in this study, such as the germline- and lysosome-related MARCM fly lines, are available upon request.

Data and code availability

- All data reported in this paper will be shared by the lead contact upon request.
- The paper does not report original code.
- Any additional information required to reanalyze the data reported in this paper is available from the lead contact upon request.

EXPERIMENTAL MODEL AND SUBJECT DETAILS

Flies were maintained on standard cornmeal/agar food at 25°C, unless otherwise noted. Flies actively used in the study were flipped to fresh food regularly to prevent the accumulation of bacteria and to maintain a consistent food source.

METHOD DETAILS

BafA treatment

Testes were dissected from age-matched young flies (under 7-days-old) in culture media (Sheng and Matunis, 2011). Culture media contained Schneider's insect medium (Gibco/Invitrogen 11720034; pH adjusted to 7.0), supplemented with 15% FBS (Sigma F3018), 0.5X penicillin/streptomycin (Gibco/Invitrogen 115140-122), and 0.2 mg/mL insulin (Sigma). All dissections were completed within 30 min of each other to ensure that the testes under analysis were removed from the body around the same time. Once dissections were completed, testes were treated with 1 μM BafA (Sigma) or DMSO (control; same dilution factor as BafA) in culture media. Testes were incubated for 24 h at 25°C in a glass dissection dish, covered with parafilm. Holes were poked in the parafilm to allow for gas exchange. After the incubation, testes were washed, fixed and stained or stained live, and then imaged (see below for staining procedures).

Immunohistochemistry

Testis immunohistochemistry was performed using standard procedures. Briefly, testes were dissected in 1X phosphate-buffered saline (PBS; 137 mM NaCl, 2.7 mM KCl, 10 mM Na_2HPO_4, 1.8 mM KH_2PO_4) and then immediately fixed in 4% paraformaldehyde. Testes were washed three times in PBT (1X PBS, 0.1% Tween-20), then incubated in blocking buffer (10% horse serum in 1X PBS) for at least 1 h at room temperature. Testes were incubated with the primary antibody diluted in blocking buffer containing 2% Triton X-100 overnight at 4°C. The next day, testes were washed five times with PBT prior to applying the secondary antibody. Testes were incubated with the secondary antibody for at least 3 h at room temperature in the dark. After the secondary antibody solution was removed, testes were washed five times with PBT. 1 μM Hoechst 33342 was incubated in the first wash to stain DNA. Testes were mounted in Vectashield antifade mounting medium prior to imaging.

LysoTracker, LysoSensor, and ProteoStat staining

LysoTracker, LysoSensor, and ProteoStat staining was performed by dissecting live testes in culture media, then immediately applying 1:1000 LysoTracker Red, 1:1000 LysoSensor Green, or 1:500 ProteoStat with 1 μM Hoechst 33342 diluted in culture media. Testes were incubated with the dye for 30 min at room temperature in the dark. After staining, testes were rinsed and mounted in culture media on a glass slide. Testes were covered with a small piece of Teflon membrane and slides were sealed with nail polish. Live imaging was performed within 1 h of dissection unless testes were cultured overnight with BafA or DMSO.

Microscopy and image processing

Images were acquired using an inverted Leica SP8 confocal microscope, equipped with a 40× objective (NA 1.30) and a white-light laser. Images were processed using Leica LAS X software, and quantifications were performed using Fiji (NIH). Imaging of LysoTracker, LysoSensor, ProteoStat, and lysosomal/endocytic vesicles was performed in live tissue, unless otherwise noted.

Testes labeled with LysoTracker were imaged at low laser power (between 1 and 3%) and gain was left at its default value. These settings over-expose dying spermatogonia at the apical tip of the testis, but allow for visualization of the transition in lysosome acidity in healthy germ cells.

Thresholding of GFP-Rho1 signal was performed using the "threshold" function in ImageJ. Images were first processed to remove noise and then images were subjected to thresholding to resolve the brightest fluorescence signal (i.e., at cell membranes).

Lysosomal area measurement

The area of an object of known size was calculated in order to calibrate measurements in ImageJ software. Once ImageJ was calibrated, Spin-GFP-positive structures (lysosomes) were outlined using the polygon selection tool. 20-30 spermatocyte lysosomes were outlined per testis, and five testes were scored per condition. The area of the outlined selections was measured once all structures had been outlined.

Quantification of germ cells missing a partitioning membrane

Z-stack images of intact live testes were acquired. Cells containing multiple nuclei that lacked a clear partitioning membrane between them and were enclosed by a common membrane were scored as germ cells missing a partitioning membrane. Testes were not squashed to prevent possible artifacts caused by the pressure of the squash. Nuclei are labeled by numbers to count individual nuclei enclosed within a single membrane. Orange numbering denotes groups of multiple nuclei without a partitioning membrane. These same annotations are used in all figures except for Figure S2G, in which nuclei are outlined (color scheme still applies), because nuclei are small and would be obscured by numbers. To determine whether nuclei that lacked one or more partitioning membranes were in the same cyst, the position of these germ cells relative to a cyst cell marker (Armadillo; Arm) was determined.

FRAP experiments

FRAP was performed using an inverted Leica DMi8 widefield microscope equipped with a 40× objective (NA 1.30). Cytosolic GFP or Ecad-GFP puncta were photobleached using a 488 nm laser at 100% power and half speed with 30 iterations. Images were acquired every 10 s for 5 min.

Aging studies

Flies were collected less than 24 h after eclosing and aged in vials on standard cornmeal/agar food at 25°C. At most, 30 flies were placed into a single vial to avoid overcrowding; vials included both males and females, such that males would continue to mate while aging. Flies were transferred to fresh food every 7–8 days. Once flies reached the appropriate age, testes were dissected and imaged.

Rapamycin feeding

For four weeks prior to testis dissection, flies were fed 10 μM rapamycin (Schinaman et al., 2019) mixed in apple juice/agar food (see CSHL "*Drosophila* apple juice-agar plates" protocol) that had been supplemented with yeast paste. Flies were maintained at 25°C and transferred to fresh food with virgin females every 3–4 days.

RNAi and mutant experiments

Male flies carrying transgenic RNAi or mutant constructs were crossed to virgin females carrying germline Gal4 transgenes. Two germline-specific Gal4 drivers were used in this study: VasaGal4 (expression in all germ cells) (Zhao et al., 2013) and BamGal4 (expression in spermatogonia at the 2-4-cell stage, but expression is maintained for the rest of development) (Chen and McKearin, 2003). Flies were incubated on standard cornmeal/agar food at 29°C for 5–7 days prior to dissection and imaging to boost Gal4 activity unless otherwise noted.

MARCM

VasaGal4; hsFLP.D5, UAS-GFP/+; FRT82B, $vha55^{j2E9}$/FRT82B, tubGal80 and VasaGal4; hsFLP.D5, UAS-GFP/+; FRT82B/FRT82B, tubGal80 males were generated via standard crossing procedures. Males were heat shocked at 37°C the same day they eclosed for 1 h to activate FLP expression and drive recombination. Following heat shock, flies were housed at 25°C on standard agar/cornmeal food until dissection. Testes were dissected and imaged live at the indicated time-points following heat shock ("clone induction").

Insoluble-protein fractionation

Following BafA/DMSO treatment, testes were lysed in NP40 buffer (6 mM Na_2HPO_4, 4 mM NaH_2PO_4, 1% NP40, 150 mM NaCl, 2 mM EDTA, 50 mM NaF, 0.1 mM Na_3VO_4, 4 μg/mL leupeptin, one Roche cOmplete™ protease inhibitor tablet, pH 7.4). Lysis was performed mechanically using a sterile pestle at room temperature. Lysates were cleared by spinning at low speed and extracted into new 1.5 mL tubes. Insoluble proteins were fractionated by centrifuging lysates at 20,000 g for 1.5 h at 4°C. The insoluble protein pellet was dissolved in detergent insoluble buffer (8 mM Urea, 2% SDS, 50 mM DTT and 50 mM Tris, pH 8) and further denatured by boiling for 10 min. Proteins were resolved by SDS-PAGE on a 4–12% Bis-Tris gel. Protein gels were stained with Coomassie Blue for 30 min and de-stained for 2–3 h in de-stain buffer (40% MeOH, 10% acetic acid) before imaging.

QUANTIFICATION AND STATISTICAL ANALYSIS

Information on sample size and statistics is provided in figure legends, where applicable. Data normality was tested via the D'Agostino-Pearson test in combination with Q-Q plots prior to performing follow-up statistical analyses using GraphPad Prism software. Statistical tests used to determine significance are indicated in figure legends. The Student's unpaired t-test was used when unpaired data for two groups were normally distributed and standard deviation was equal between both groups. Welch's unpaired t-test was used when unpaired data for two groups were normally distributed, but standard deviation was not equal. The Mann-Whitney U-test was used when unpaired data for two groups were not normally distributed. The paired t-test was used when paired data for two groups were normally distributed and standard deviation was equal. The Wilcoxon matched pairs signed rank test was used when paired data for two groups were not normally distributed. The Brown-Forsythe ANOVA with Dunnett's multiple comparisons test was used when there were more than two groups with normally distributed data, but standard deviation was not equal between the groups.